Title

Nonequilibrium Ionic Response of Biased Mechanically Controllable Break Junction (MCBJ) Electrodes

Journal

The Journal of Physical Chemistry C, 118(7)

ISSN

1932-7447

Authors

Doi, Kentaro
Tsutsui, Makusu
Ohshiro, Takahito
et al.

Publication Date

2014-02-20

DOI

10.1021/jp409798t

Peer reviewed

THE JOURNAL OF PHYSICAL CHEMISTRY C

Article

pubs.acs.org/JPCC

Nonequilibrium Ionic Response of Biased Mechanically Controllable Break Junction (MCBJ) Electrodes

Kentaro Doi,*[,†] Makusu Tsutsui,[‡] Takahito Ohshiro,[‡] Chih-Chun Chien,[§] Michael Zwolak,[∥] Masateru Taniguchi,*[,‡] Tomoji Kawai,[‡] Satoyuki Kawano,*[,†] and Massimiliano Di Ventra*[,⊥]

[†]Department of Mechanical Science and Bioengineering, Graduate School of Engineering Science, Osaka University, Toyonaka, Osaka 560-8531, Japan

[‡]The Institute of Scientific and Industrial Research, Osaka University, Ibaraki, Osaka 567-0047, Japan

[§]Theoretical Division, Los Alamos National Laboratory, Mail Stop B213, Los Alamos, New Mexico 87545, United States

[∥]Department of Physics, Oregon State University, Corvallis, Oregon 97331, United States

[⊥]Department of Physics, University of California, San Diego, La Jolla, California 92093, United States

ABSTRACT: Novel experimental techniques allow for the manipulation and interrogation of biomolecules between metallic probes immersed in micro/nanofluidic channels. The behavior of ions in response to applied fields is a major issue in the use of these techniques in sensing applications. Here, we experimentally and theoretically elucidate the behavior of background currents in these systems. These large currents have a slowly decaying transient response, as well as noise that increases with ionic concentration. Using mechanically controllable break junctions (MCBJ), we study the ionic response in nanogaps with widths ranging from a few nanometers to millimeters. Moreover, we obtain an expression for the ionic current by solving time-dependent Nernst−Planck and Poisson equations. This expression shows that after turning on an applied voltage, ions rapidly respond to the strong fields near the electrode surface, screening the field in the process. Ions subsequently translocate in the weak electric field and slowly relax within the diffusion layer. Our theoretical results help to explain the short- and long-time behavior of the ionic response found in experiments, as well as the various length scales involved.

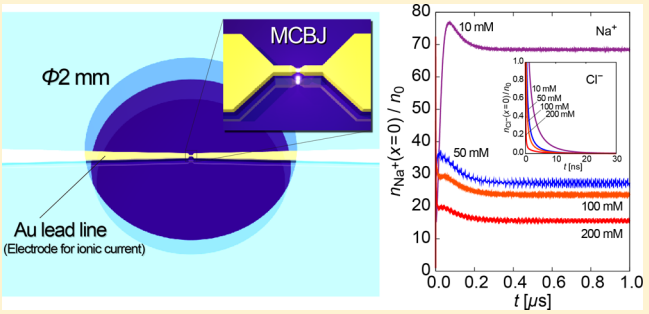

INTRODUCTION

The dynamics of ions in electrolyte solutions is receiving renewed interest due to the appearance of novel sensing applications, such as single-molecule approaches to sequencing based on micro/nanofluidic devices.[1−4] As part of this general platform, several studies, for instance, measured the tunneling current across individual nucleotides using a mechanically controllable break junctions (MCBJ).[5−9] Other recent works developed ionic current rectifiers that operate by exploiting surface charge effects,[10−12] including devices that can be reconfigured by the application of external fields.[13] Moreover, another pioneering work investigated the ionic response to ac fields.[14] From another perspective, there are many possibilities for constructing narrow channels to obtain various nonlinear ionic transport characteristics. Despite a long history,[15−18] however, the relation between the time and spatial scales of the electrical response of ionic solutions at the nanoscale remains unsolved. This is a key issue in controlling ionic transport by externally applied dc or ac fields. Its study is also of relevance for any nanofluidic technology that employs electrodes in solution, e.g., for enhancing the energy storage of electrochemical capacitors[19−21] and for solid-state nanopore technologies[22−25] in which electrical probes interrogate translocating molecules.[26−29] In such complex systems, current noise is also inevitable due to the presence of ions and this noise obscures the electrical signals of interest − the ones from the individual molecules. A full understanding of the mechanisms responsible for the behavior of these "background" currents is therefore needed, as it will help the development of single-molecule approaches to sequencing based on electronic transport.[30]

In this study, we develop a combined experimental and theoretical understanding of the transient electrical response of ions in the vicinity of biased electrodes that have several associated length scales, such as the MCBJ electrodes shown in Figure 1a. This system displays a slowly decaying transient current and an associated noise that increases with the ionic concentration. We demonstrate a useful computational method to treat the various length and time scales involved in this complex phenomenon. The resulting theoretical understanding reveals the rich behavior in the electrochemical response of ions between nanoelectrodes.

Received: October 2, 2013
Revised: January 16, 2014
Published: January 18, 2014

   dx.doi.org/10.1021/jp409798t | J. Phys. Chem. C 2014, 118, 3758−3765

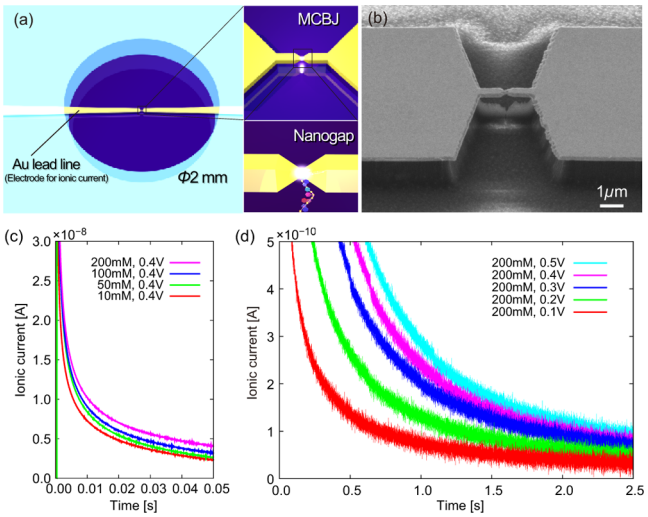

Figure 1. (a) Schematic illustration and (b) SEM image of MCBJ electrodes, (c) transient current response of NaCl solution under an applied potential of 0.4 V for several salt concentrations, and (d) current response for a concentration of 200 mM NaCl at various voltages. Data from applied voltages above 0.5 V are omitted here for clarity, although all data ranging from 0.1 to 0.9 V are summarized in Table 1. After an initial rapid increase, the ionic current then slowly decays (with a time scale of about 1 s, Table 1).

EXPERIMENTAL SECTION

Parts a and b of Figure 1 show a schematic illustration and scanning electron microscopy (SEM) image, respectively, of a MCBJ made with Au electrodes. The lithographically defined nanojunction is fabricated on a polyimide-coated phosphor bronze substrate. It consists of 30 nm thick Au/Cr wires of approximately 10 mm end-to-end length and width tapered from 10 to 1 μm along the length. We create a pair of nanoelectrodes using a self-breaking technique,[5] which forms a 1 nm electrode gap with atomically sharp Au tips sensitive enough to detect single molecules by a tunneling current.[7−9] In our experimental setup, the electrodes are symmetrically placed in a liquid container of 2 mm diameter. Therefore, large surfaces ($\sim 10^{-8}$ m^2) of the lead line are exposed to the electrolyte solution, which cause the background current with noise, as shown in Figure 1c. NaCl aqueous solution is prepared by dissolving NaCl salt in Milli-Q water. To investigate the dependence of transient ionic currents on applied voltages and molarities, NaCl solutions (1, 10, 50, 100, and 200 mM) are prepared and time transition profiles are measured under a constant dc voltage ranging from 0.1 to 0.9 V. Here, the electrical response of NaCl solution is measured for various salt concentrations under constant dc voltage with a sampling frequency of 10 kHz by using a custom-built logarithmic current amplifier and a PXI-4071 digital multimeter (National Instruments).[9] In this study, NaCl solution is employed to clearly separate the transport of Na^+ and Cl^-, although KCl may be better as an electrolyte to yield high conductivity of ionic currents. From Figure 1c,d, the transient response displays a rapid increase and subsequent slow decay of the ionic current. The time constant is evaluated by least-squares fit and summarized in Table 1. Particularly, the time constant increases with increasing molarity and applied potential and is on the order of 1 s for the parameter regimes studied. Assuming an equivalent circuit, this system would then consist of a 1 GΩ resistance evaluated from the current−voltage characteristics and a 1 nF capacitor. However, such a huge resistance and small capacitance in the narrow space cannot be explained by the conventional macroscopic models. We now seek to understand these features by employing a microscopic model.

THEORETICAL MODEL

A large number of previous works sought to understand electrochemical reactions at electrode surfaces,[31−36] ionic motions in solutions,[37,38] and dynamical response.[39,40] In recent years, the nonequilibrium behavior of ions confined to micro/nanoscale spaces is becoming increasingly important. Here, we focus on phenomena outside the strongly adsorbed (Stern) layer.[41] Ionic motion in aqueous solution is expressible in terms of Newton's equation of motion with fluctuations and dissipation, which gives $m\dot{v} = \xi v + F + R$, where m is the mass, v is the velocity, ξ is the friction coefficient, F is the external force (due to an applied potential), and R is the random force from the solvent molecules. In this scenario, ions will rapidly respond to the application of an applied potential, strongly screening it by building up near the electrode surfaces.[35,37,42,43] Subsequently, ions gradually form a diffusion layer.

We elucidate the scale of this phenomena (and hence illuminate the underlying physics) by considering one-dimensional ionic current densities $j_i(x,t)$ due to the migration and diffusion of each of the ionic species i in aqueous solution. Taking into account the stochastic process in electrolyte solutions, ionic motions are expressible by a Nernst−Planck equation for each species:[15,16,41,44]

$$\frac{\partial \rho_i}{\partial t} = -\frac{\partial j_i}{\partial x} \qquad j_i(x,t) = \frac{F_i}{\xi_i}\rho_i - D_i\frac{\partial \rho_i}{\partial x} \tag{1}$$

where $\rho_i(x,t)$ is the charge density expressed by the valence z_i, the number density $n_i(x,t)$, and the elementary charge e: $\rho_i = z_i e n_i$, and D_i is the diffusion coefficient. The coordinate x is defined in an interval of $x \in (0, L)$ where the electrode surface is at $x = 0$ and the thickness of the diffusion layer is L. Ionic migration is driven by the electrostatic force due to the applied potential and thus F_i can be represented by the gradient of potential ϕ such that $F_i = -z_i e\nabla\phi$. The relation between ϕ and ρ_i is expressed by the Poisson equation:

$$-\varepsilon\Delta\phi = \sum_i \rho_i \tag{2}$$

Table 1. Time Constant τ of Ionic Current Response

condition	τ [s]	condition	τ [s]	condition	τ [s]
1 mM/0.4 V	0.459	200 mM/0.1 V	0.267	200 mM/0.6 V	0.544
10 mM/0.4 V	0.499	200 mM/0.2 V	0.446	200 mM/0.7 V	0.558
50 mM/0.4 V	0.556	200 mM/0.3 V	0.528	200 mM/0.8 V	0.599
100 mM/0.4 V	0.594	200 mM/0.4 V	0.542	200 mM/0.9 V	0.710
		200 mM/0.5 V	0.577		

dx.doi.org/10.1021/jp409798t | J. Phys. Chem. C 2014, 118, 3758−3765

where ε is the dielectric constant. The solution with respect to charge distributions is given by

$$\phi(x) = \phi(0) + (\phi(L) - \phi(0))\frac{x}{L} + \frac{1}{\varepsilon}\left(1 - \frac{x}{L}\right)\sum_i \int_0^x x'\rho_i(x')\,dx' + \frac{x}{\varepsilon}\sum_i \int_x^L \left(1 - \frac{x'}{L}\right)\rho_i(x')\,dx' \quad (3)$$

where $\phi(0)$ and $\phi(L)$ are the potentials at $x = 0$ and L, respectively. The summation is taken for all species that contribute to ϕ. The ion density and the electrostatic potential should be determined self-consistently to solve the nonlinear partial differential equation. In previous works, Sokalski et al.[44,45] and Lingenfelter et al.[46] developed numerical methods for the coupled Nernst−Planck and Poisson equations and obtained useful results for the ion selective membrane potentials. In particular, they discuss a long-period response at the interface of the electrolyte solution and an ion-exchange membrane. Here, focusing on MCBJ electrodes, we introduce another method that correctly predicts the rapid response and noise found in experiments (Figure 1c,d). Incorporating source terms into the dynamics, eq 1 becomes

$$\frac{\partial \rho_i}{\partial t} - \frac{z_i e}{\xi_i}\frac{\partial}{\partial x}\left(\frac{d\phi}{dx}\rho_i\right) - D_i\frac{\partial^2 \rho_i}{\partial x^2} = \sum_r f_{ir}\cos(\omega_{ir}t + \varphi_{ir})\delta(x) \quad (4)$$

where f_{ir} are constants depending on the current density and noise, and φ_{ir} are the phase shifts at $t = 0$. In the numerical solution, ϕ depends only on the displacement of ions and thus it is treated as independent of time in the short interval. The smallest time step, which is large enough to represent the stochastic process, should be determined properly to maintain constraints at boundaries and electroneutrality. The source terms can express noise generated at $x = 0$, which induces external flux in the domain. As a first step, we consider Gaussian white noise, although it is known that noise detected in micro/nanofluidic devices usually also show flicker noise.[47−49] The parameters ω_{ir} and φ_{ir} are generated by Gaussian[50] and uniform probability distributions, respectively.

Rescaling x, t, and ϕ to make them dimensionless by

$$x^* = \frac{x}{L} \qquad t^* = \frac{D_i}{L^2}t \qquad \psi_i^* = \frac{z_i e\phi}{D_i\xi_i} = \frac{z_i e\phi}{k_B T} \quad (5)$$

and, considering a unit surface, replacing ρ_i by

$$n_i^* = \frac{L}{z_i e}\rho_i \exp\left[\frac{1}{2}\int^{x^*}\frac{d\psi_i^*}{dx^{*\prime}}\,dx^{*\prime}\right] \quad (6)$$

eq 4 becomes

$$\left[\frac{\partial}{\partial t^*} + \frac{1}{4}\left(\frac{d\psi_i^*}{dx^*}\right)^2 - \frac{1}{2}\frac{d^2\psi_i^*}{dx^{*2}} - \frac{\partial^2}{\partial x^{*2}}\right]n_i^* = \exp\left[\frac{1}{2}\int^{x^*}\frac{d\psi_i^*}{dx^{*\prime}}\,dx^{*\prime}\right]\sum_r f_{ir}^*\cos(\omega_{ir}^* t^* + \varphi_{ir})\delta(x^*) \quad (7)$$

where $f_{ir}^* = L^2 f_{ir}/z_i e D_i$ and $\omega_{ir}^* = L^2\omega_{ir}/D_i$. For the other species, the equation can be derived in the same manner. Here, n_i^* and ψ_i^* are expanded by the Fourier series:

$$n_i^*(x^*,t^*) = \sum_k c_{ik}(t^*)e^{ik\pi x^*} \quad (8)$$

$$\psi_i^*(x^*) = \sum_k g_{ik}e^{ik\pi x^*} \quad (9)$$

where $k = 0, \pm1, \pm2, \ldots$, $\delta(x^*)$ is also expanded similarly:

$$\delta(x^*) = \frac{1}{2L}\sum_k e^{ik\pi x^*} \quad (10)$$

Each basis function is orthogonal on $x^* \in [-1, +1]$. In this model, a mirror symmetry is assumed at $x^* = 0$ and 1. Ions are adsorbed or reflected at $x^* = 0$ and the concentrations correspond to those of bulk at $x^* \geq 1$, conserving the electroneutrality in the domain. On the basis of the description above, eq 7 becomes

$$\frac{d\mathbf{c}_i}{dt^*} + \hat{H}_i\mathbf{c}_i = \frac{1}{2}\sum_r f_{ir}^*\cos(\omega_{ir}^* t^* + \varphi_{ir}) \quad (11)$$

where

$$H_{ikl} = \pi^2 k^2\delta_{k,l} + \frac{\pi^2}{2}(k-l)^2 g_{i(k-1)} - \frac{\pi^2}{4}\sum_{k_1} k_1(l-k-k_1)g_{\{ik_1\}}g_{i(k-l+k_1)} \quad (12)$$

$\Psi_i^*$are real functions and thus $\hat{H}_i$ are Hermitian matrices. The variable transform of eq 6 results in equations amenable to analytic treatment. For the homogeneous case, we can solve eq 11 via its eigenvalues λ_{ij} and eigenvectors. Using these solutions, we can also solve the inhomogeneous case. If λ_{ij} are nonzero, then

$$c_{ik}(t^*) = \frac{1}{2}\sum_j\sum_l u_{kj}^\dagger u_{jl}\left[\frac{f_{ir=0}^*}{\lambda_{ij}}(1 - e^{-\lambda_{ij}t^*})\cos\varphi_{ir=0} + \sum_{r\neq 0} f_{ir}^* I_{ir}^j(t^*)\right] + \sum_j\sum_l u_{kj}^\dagger u_{jl}c_{il}^0 e^{-\lambda_{ij}t^*} \quad (13)$$

where $u_{kj}^\dagger$ are the conjugate transpose of u_{jk}, c_{il}^0 are constants determined at the initial condition and

$$I_{ir}^j(t^*) = e^{-\lambda_{ij}t^*}\int_0^{t^*}\cos(\omega_{ir}^* t^{*\prime} + \varphi_{ir})e^{\lambda_{ij}t^{*\prime}}\,dt^{*\prime} \quad (14)$$

At equilibria, λ_{ij} should be zero. As a consequence, we obtain

$$\rho_i(x,t) = \frac{z_i e}{L}\exp\left[-\frac{z_i e}{2k_B T}\int^x\frac{d\phi}{dx'}\,dx'\right]\sum_k c_{ik}\exp\left[i\frac{k\pi x}{L}\right] \quad (15)$$

and, from eq 1,

$$j_i(x,t) = \frac{2\pi z_i e D_i}{L^2}\exp\left[-\frac{z_i e}{2k_B T}\int^x\frac{d\phi}{dx'}\,dx'\right] \times \sum_{k>0} k\,\mathrm{Im}\left\{c_{ik}\exp\left[i\frac{k\pi x}{L}\right]\right\} - \frac{z_i e D_i}{2k_B T}\frac{d\phi}{dx}\rho_i \quad (16)$$

The nonlinear eq 7 can be numerically solved according to the procedure shown in Figure 2.

The one-dimensional coordinate space is divided into 2^n points where $n \geq 7$ is employed to maintain the numerical

dx.doi.org/10.1021/jp409798t | J. Phys. Chem. C 2014, 118, 3758−3765

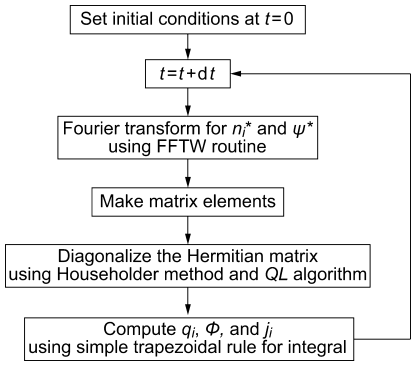

Figure 2. Flowchart of numerical analysis.

accuracy. Computations are carried out for L = 2, 5, 10, 15, and 20 nm with a 128 grid and for L = 30 and 40 nm with a 256 grid to evaluate eigenvalues of the homogeneous equation of eq 7. Furthermore, for the inhomogeneous case with the source and noise, the computations are carried out for L = 40 nm with a 256 grid. In each case, the time step is fixed at $dt = 1 \times 10^{-11}$ s to maintain the computational accuracy of ρ_i and ϕ. From the viewpoint of stochastic processes, the condition of $dt < 10^{-11}$ s tends to cause the divergence of computations. On the other hand, large dt cannot represent electronic properties precisely. In the numerical analysis, ω_{ir} are determined randomly by the Box–Muller[50] algorithm and φ_{ir} by a uniform random number in $(-\pi/2, +\pi/2)$. The variance of Gaussian white noise is set to $(1 \times 10^{12})^2$. In this study, the number of noise components is set to 100.

RESULTS AND DISCUSSION

We apply this model to evaluate the ionic current near an Au electrode in NaCl solution. At the negatively charged cathode surface, Na^+ is highly concentrated regardless of the anion species. In the numerical analysis, L is taken as a constant for each molarity. The applied potential is restricted to a practical range of potentials in aqueous solution: $\phi(0) = -0.01$ to -1 V and $\phi(L) = 0$ V. The valence is +1 and −1 for Na^+ and Cl^-, respectively. The diffusion coefficients are known: $D_{Na^+} = 1.35 \times 10^{-9}$ m^2/s and $D_{Cl^-} = 2.03 \times 10^{-9}$ m^2/s.[38] The dielectric constant and temperature are $\varepsilon = 78.4\varepsilon_0$,[51] where ε_0 is the dielectric constant of vacuum and T = 298.15 K, respectively. As a first approximation, the time constant $\tau = L^2/D\lambda$ due to the slowest process within the transient response is determined by the homogeneous equation of eq 7 for the two component system.

Figure 3 shows τ for Na^+ and Cl^- as a function of the ratio of $V = \phi(L) - \phi(0)$ to L for the molarity of 1, 10, 50, and 100 mM, where V/L merely expresses a fraction of the applied potential and the length, but not the actual electric field in the system. It is found that τ tends to be proportional to $(V/L)^{\zeta}$, where $\zeta = -2.15$ for Na^+ and -2.05 for Cl^- resulting from the fits of the computational data at 1 mM. We can then predict that $\tau \propto (V/L)^{-2}$ in the dilute limit, because the second term on the left-hand side of eq 7 dominates as $n_i^* \sim 0$. On the other hand, the gradient decreases as the molarity increases due to the strong screening of the electrode surface. These results suggest that ions rapidly respond to the strong electric field near the electrode surface and that τ becomes large in the weak electric fields far away from the electrode. The magnitude of τ is expected to be on the order of 1 s for the electric field of 10^3 V/m. Thus, L is estimated to be 100 μm (1 mm), when the

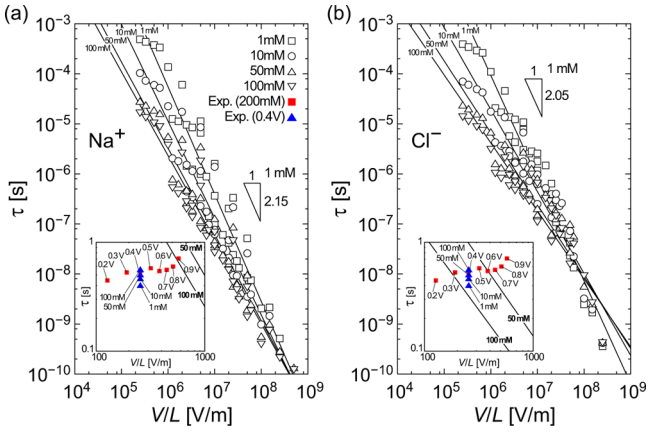

Figure 3. Time constant τ of the transient response of (a) Na^+ and (b) Cl^- in aqueous solution as a function of (V/L) where $V = \phi(L) - \phi(0)$. τ and V/L show $\tau \propto (V/L)^{-2.15}$ for Na^+ and $\tau \propto (V/L)^{-2.05}$ for Cl^- fitting the computational data at 1 mM. Experimental results (Figure 1c,d) are also shown in insets.

applied potential is on the order of 0.1 V (1 V). Recently, a similar trend of time and spatial scales of the ionic response was reported by using a nanofluidic field effect transistor.[14] In experimental systems, as shown in Figure 1a, several length scales are usually present, but the slowest process is likely the result of the longest length scale. To evaluate τ from the experimental results (Figure 1c,d), L is fixed at 1.57 mm assuming that the longest length along the electric field line in the experimental system is a quarter of 1 mm radius circle, although the actual diffusion layer thickness is possibly less than this value. The series of τ from the experiment with 200 mM solution is expected to show a negative gradient if L becomes larger with increasing applied potential. Consequently, the theoretical evaluations are in reasonable agreement with the experimental results.

To discuss the spatial scale of the ionic response, the time evolution of the ionic current and density at the surface are calculated for various L with respect to applied potentials. A constant source term, on the right-hand side of eq 7, is applied only for Na^+ to define a steady current condition. We set $f_{Na^+ r=0} = -\alpha e^2 n_0 D(\phi(L) - \phi(0))/Lk_BT$ on the basis of the Nernst–Einstein relation, where n_0 is the number density of bulk solution and α is a constant. Here, we demonstrate a case of $\alpha = 1$. The total ionic current density is evaluated as $\sum_i(j_i(x\to0) - j_i(x\to L))$, which is simply the difference of ion flux at both ends without any electrochemical reaction at the electrode surface. Figure 4 shows the time evolution of net current density and normalized number density of Na^+ at the cathode surface, resulting from the condition of L = 5 and 20 nm under the applied potential of V = 0.05 V. In both lengths of L, the current density increases and converges to a constant value that becomes higher with the molarity, as shown in Figure 4a,c. The response of the current density is apparently affected by the density of Na^+. As shown in Figure 4b, it is interesting that the fractional density of Na^+ relatively increases up to 100 mM and then decreases with increasing the molarity when L = 5 nm. On the other hand, the normalized density seems to uniformly decrease with increasing molarity when L = 20 nm (Figure 4d). This means that there is an absolute limit of the surface density with respect to V and L. The response time becomes longer with increasing L. It is then suggested that it takes long times when there is a large space for ions to stabilize the electric field

dx.doi.org/10.1021/jp409798t | J. Phys. Chem. C 2014, 118, 3758–3765

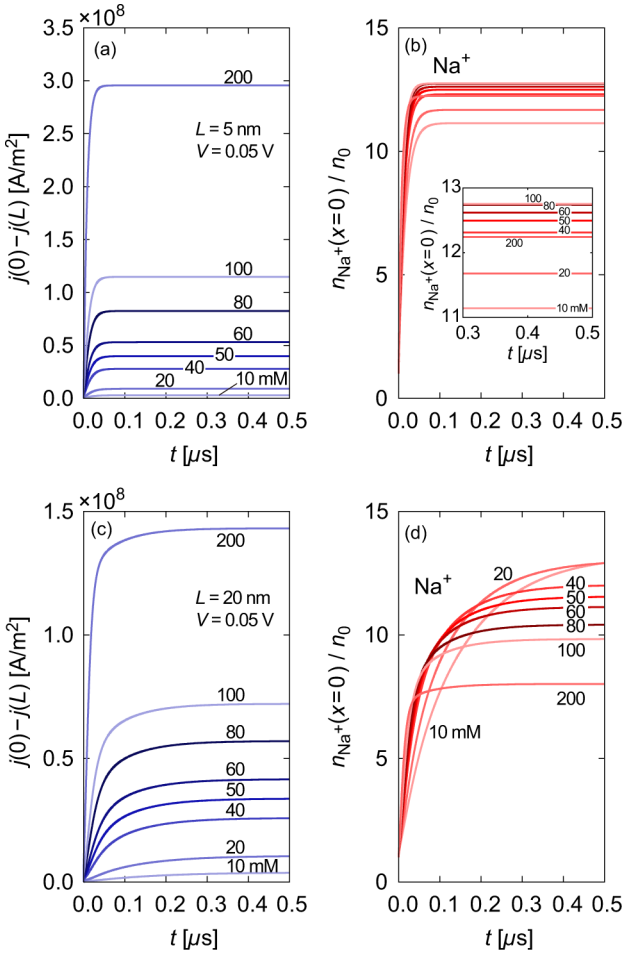

Figure 4. Time evolution of net current density $(j(0) - j(L))$ and normalized number density of Na^+ at $x = 0$ under applied electric potential of $V = \phi(L) - \phi(0) = 0.05$ V. (a) and (b) are respectively the current density and the normalized density (magnfied view in inset) for $L = 5$ nm, and (c) and (d) are similarly for $L = 20$ nm. Molarity dependence is presented ranging from 10 to 200 mM.

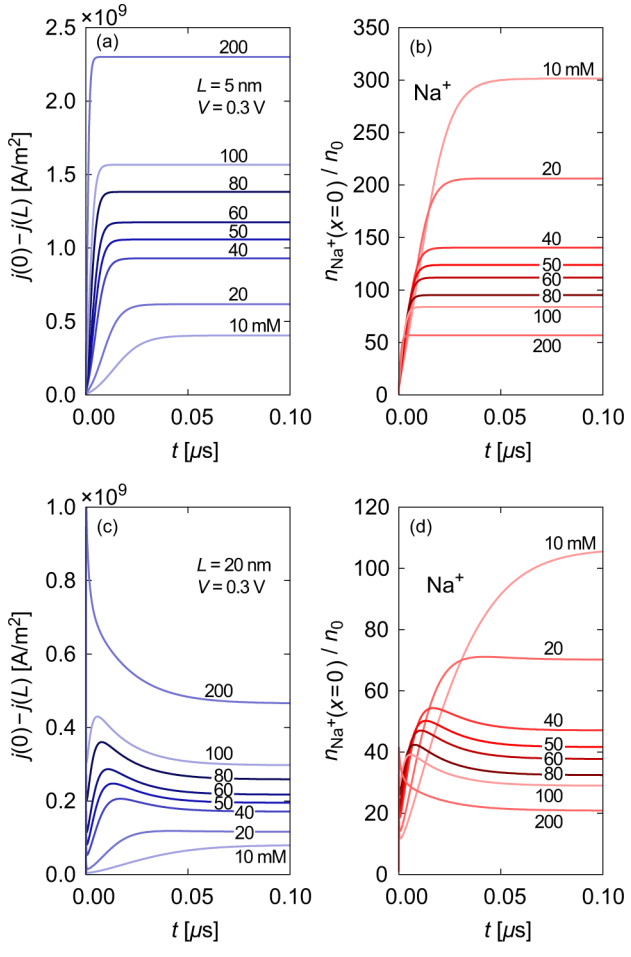

Figure 5. Time evolution of net current density $(j(0) - j(L))$ and normalized number density of Na^+ at $x = 0$ under applied electric potential of $V = \phi(L) - \phi(0) = 0.3$ V: (a), (b) for $L = 5$ nm and (c), (d) for $L = 20$ nm, in the same manner as Figure 4.

in solution. Figure 5 also shows similar computational results for the applied potential of $V = 0.3$ V. As shown in Figure 5a, the current density quickly increases and is saturated at a steady state, when the bulk solution is defined at $L = 5$ nm. The response time becomes shorter with increasing the molarity. As shown in Figure 5b, the response of surface density is correlated with the current density and the difference from the bulk tends to be apparent at low concentrations. On the other hand, clear peaks can be observed in the ionic current response as L increases.

As shown in Figure 5c, a peak point can be recognized at 40 mM and turns to be a sharp one as the molarity increases. The surface density of Na^+ exhibits a similar response (Figure 5d). It is found that the small L causes a sufficient provision of Na^+ near the cathode that results in quickly charging and stabilizing the surface. This property may be preferable to make a good capacitor, but such a trend was not observed in experiments. On the other hand, the large L results in the appearance of maximum peak in the response, in which Na^+ highly concentrates at the electrode surface immediately after applying an electric potential and successively reduces to relax the excessive concentration. Additionally, it is clear that the magnitude of applied potentials also causes the response characteristics, in comparison with Figure 4.

In the next step, to replicate noise associated with electrochemical reactions,[35,42] we then apply other source terms on the right-hand side of eq 7. Perturbations at the cathode surface $(x = 0)$ due to charge transfer via electrochemical reactions are mimicked by the frequency-dependent sources. The amplitude of noise is determined to be proportional to the square root of the bulk density based on the surface charge density[41] such that $f_{Na^+r} = \beta\eta {n_0}^{1/2}$ with a constant β common to each molarity. η is determined from $f_{Na^+r=0}$ of 10 mM such that $\eta = -f_{Na^+r=0}/\alpha {n_0}^{1/2}$, because in this study, the molarity of 10 mM is the minimum and available as a reference. Details of electrochemical reactions have not been explicitly represented in the framework of Nernst−Planck equation. Here, we suggest a mathematical model to mimic such perturbations, although the quantitative evaluation of noise remains to be solved. We perform computations for a case of $\alpha = 1$, $\beta = 100$, $L = 40$ nm, and $V = 0.3$ V. Figure 6 shows current density and normalized number density of each species obtained from 10, 50, 100, and 200 mM NaCl solutions as a function of time. As shown in Figure 6a, the net current density rapidly increases at the moment when the electric potential is applied. The maximum peak appears to be higher as the molarity increases, associated with the increase of Na^+ at

dx.doi.org/10.1021/jp409798t | J. Phys. Chem. C 2014, 118, 3758−3765

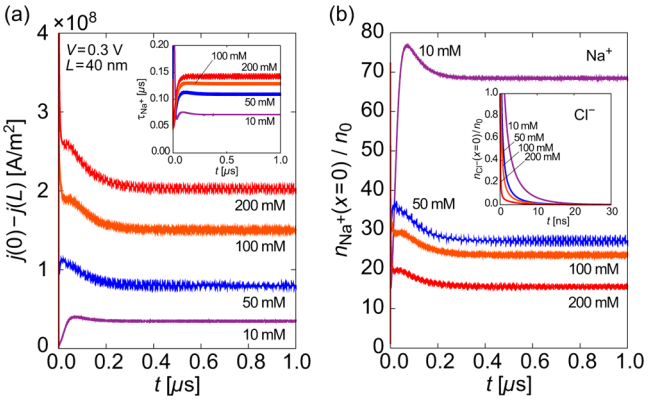

Figure 6. Time evolution of (a) current density of 10 (purple), 50 (blue), 100 (orange), and 200 (red) mM NaCl solution where τ of Na^+ is also shown in the inset and (b) normalized number density of Na^+ and Cl^- (inset) at $x = 0$. Computations are for $V = 0.3$ V and $L = 40$ nm.

the cathode surface (Figure 6b). Such tendencies are similar to those in Figure 5c,d. Furthermore, the time constant τ of Na^+ tends to become large as the molarity increases as shown in the inset of Figure 6a. This trend has never been observed with short L. The time scale $\tau \sim 0.1$ μs, obtained from $L = 40$ nm and $V = 0.3$ V ($V/L \sim 10^7$V/m), closely corresponds to the result from Figure 3. This result explains well the experimental observations (Figure 1c,d and Table 1). Cl^- also shows large τ but does not contribute to the current density at the cathode side due to the extremely low density near the surface. As shown in Figure 6b, the response in the current density is obviously caused by the prominent increase and subsequent decrease of Na^+ at the surface. Furthermore, the noise propagating through the solution is suppressed due to the highly screened surface. This is a reason why the effect of noise seems to be weakened as the molarity increases, even though the noise is proportional to the square root of bulk concentration.

Figure 7 shows the density profiles of Na^+, Cl^-, the electrostatic potential, and the electric field obtained from the simulations. Parts a–c, d–f, g–i, and j–l of Figures 7 present results from 10, 50, 100, and 200 mM NaCl solutions, respectively. Resulting from the density of Na^+, the electrode surface is strongly screened and the diffusion layer is gradually formed as time passes. On the other hand, the distribution of Cl^- rapidly decreases near the electrode surface and exhibits uniform increase as a function of x in each molarity. The electrostatic potential shows a drastic increase near the electrode surface and the screening effect is apparent as the molarity increases. These trends are also expressed more clearly by the electric field strength. As previously discussed for Figures 4 and 5, high salt concentrations may cause a rapid response to the applied field especially near the electrode surface and thus weak fields remain behind the strongly screened surface, which cause the whole solution to take a long period to relax.

Figure 8a shows density distributions of Na^+ at $t = 1.0$ μs. For each concentration, a minimum peak of Na^+ is found near the surface. This peak implies that part of the ions tends to adsorb on the electrode surface and the others separate, forming density gradients. In the case of Cl^- as shown in Figure 8b, the concentration is depleted near the electrode surface and approaches its bulk density as x increases. Due to these distributions, the electrostatic potentials show extremely steep

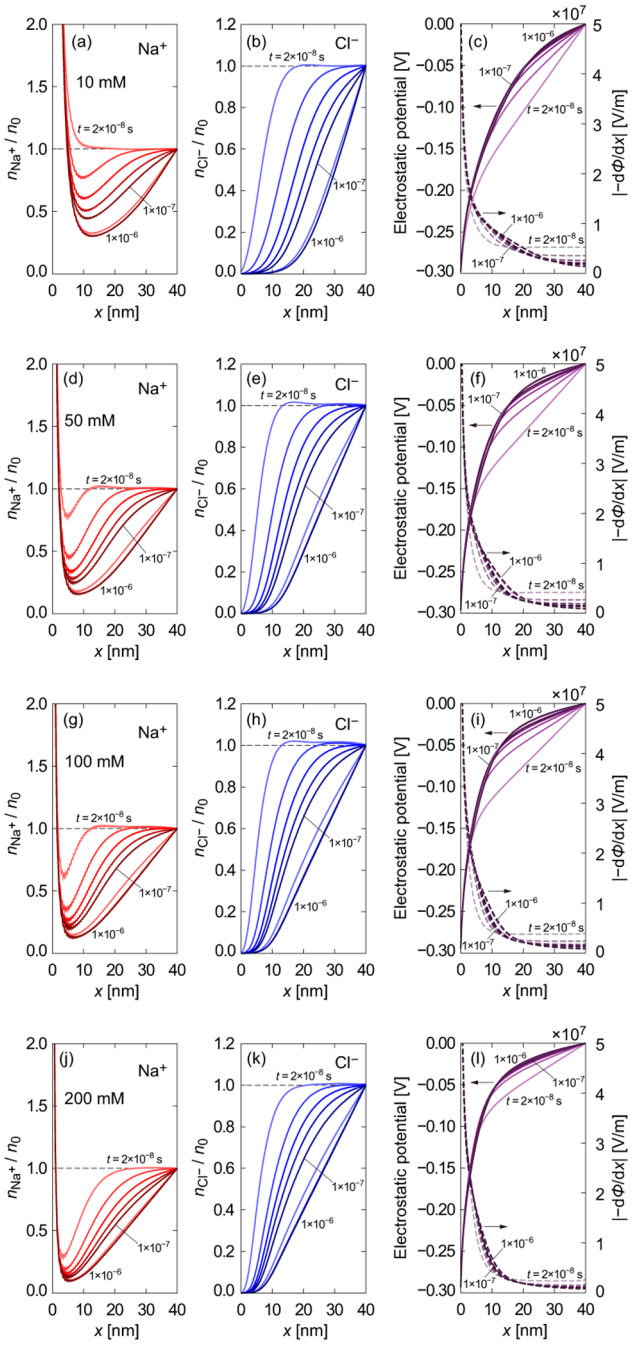

Figure 7. Time transition of number densities, electrostatic potential, and electrostatic field resulting from (a)–(c) 10 mM, (d)–(f) 50 mM, (g)–(i) 100 mM, and (j)–(l) 200 mM NaCl solutions, applying $V = 0.3$ V on the length of $L = 40$ nm.

gradients near the electrode surface, as shown in Figure 8c. In the 100 and 200 mM solutions, the electric field strength is 2 orders of magnitude different between the two ends. Despite the strong screening, however, weak fields also seem to exist widely in the solution, which drives the transport of electrolytes.

CONCLUSIONS

In this study we developed a theoretical model and carried out numerical calculations to explain the dynamical behavior of electrolytes near biased electrodes in nanofluidic devices. We have found that the ionic response strongly depends on the

dx.doi.org/10.1021/jp409798t | J. Phys. Chem. C 2014, 118, 3758–3765

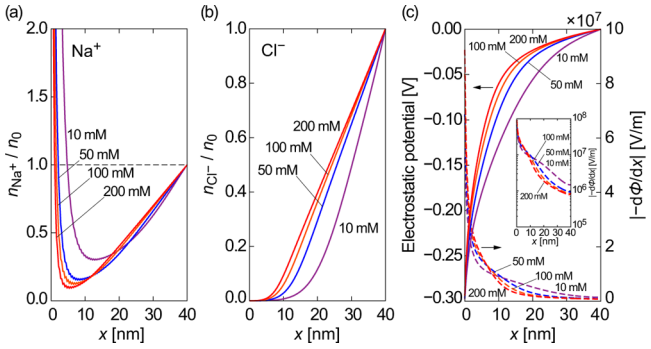

Figure 8. Normalized density distribution of (a) Na^+ and (b) Cl^- for 10 (purple), 50 (blue), 100 (orange), and 200 (red) mM and (c) the electrostatic potential (solid line) and the electric field strength (dashed line) that is also shown in logarithmic scale in the inset. These characteristics are obtained from data at t = 1.0 μs.

applied potential and the length of the nanogap, from which an effective power law arises in the numerical calculations. Moreover, multiple time and length scales are involved in the ionic response to a biased nanogap with large electrode surfaces as is present in MCBJ systems. The power law behavior shown in Figure 3 will allow for the prediction of the response times in devices and future experiments. Furthermore, this work is an important building block to investigate multiple electrode systems—a problem that requires a solution in higher dimensions where efficient computational techniques are required. These findings will also be helpful in understanding the background currents in novel single-molecule sequencing approaches, as well as the behavior of electrochemical capacitors for high-energy density storage.

AUTHOR INFORMATION

Corresponding Authors

*K. Doi: phone, +81 6 6850 6178; e-mail, doi@me.es.osaka-u.ac.jp.
*M. Taniguchi: phone, +81 6 6879 8446; e-mail, taniguti@sanken.osaka-u.ac.jp.
*S. Kawano: phone, +81 6 6850 6175; e-mail, kawano@me.es.osaka-u.ac.jp.
*M. Di Ventra: phone, +1 858 822 6447; e-mail, diventra@physics.ucsd.edu.

Notes

The authors declare no competing financial interest.

ACKNOWLEDGMENTS

This work was partly supported by the Japan Society for the Promotion of Science (JSPS) through its "Funding Program for World-Leading Innovative R&D on Science and Technology". C.C.C. acknowledges the support of the U.S. DOE through the LANL/LDRD Program and M.D. partial support from NIH.

REFERENCES

(1) Zwolak, M.; Di Ventra, M. Colloquium: Physical Approaches to DNA Sequencing and Detection. *Rev. Mod. Phys.* **2008**, *80*, 141−165.
(2) Branton, D.; et al. The Potentila and Challenges of Nanopore Sequencing. *Nat. Biotechnol.* **2008**, *26*, 1146−1153.
(3) Howorka, S.; Siwy, Z. Nanopore Analytics: Sensing of Single Molecules. *Chem. Soc. Rev.* **2009**, *38*, 2360−2384.
(4) Venkatesan, B. M.; Bashir, R. Nanopore Sensors for Nucleic Acid Analysis. *Nat. Nanotechnol.* **2011**, *6*, 615−624.
(5) Tsutsui, M.; Shoji, K.; Taniguchi, M.; Kawai, T. Formation and Self-Breaking Mechanism of Stable Atom-Sized Junctions. *Nano Lett.* **2008**, *8*, 345−349.
(6) Tsutsui, M.; Taniguchi, M.; Kawai, T. Fabrication of 0.5 nm Electrode Gaps Using Self-Breaking Technique. *Appl. Phys. Lett.* **2008**, *93*, 163115.
(7) Tsutsui, M.; Taniguchi, M.; Kawai, T. Transverse Field Effects on DNA-Sized Particle Dynamics. *Nano Lett.* **2009**, *9*, 1659−1662.
(8) Tsutsui, M.; Taniguchi, M.; Yokota, K.; Kawai, T. Identifying Single Nucleotides by Tunnelling Current. *Nat. Naotechnol.* **2010**, *5*, 286−290.
(9) Ohshiro, T.; Matsubara, K.; Tsutsui, M.; Furuhashi, M.; Taniguchi, M.; Kawai, T. Single-Molecule Electrical Random Resequencing of DNA and RNA. *Sci. Rep.* **2012**, *2*, 501 DOI: 10.1038/srep00501.
(10) Karnik, R.; Duan, C.; Castelino, K.; Daiguji, H.; Majumdar, A. Rectification of Ionic Current in a Nanofluidic Diode. *Nano Lett.* **2007**, *7*, 547−551.
(11) Vlassiouk, I.; Siwy, Z. S. Nanofluidic Diode. *Nano Lett.* **2007**, *7*, 552−556.
(12) Nam, S.-W.; Rooks, M. J.; Kim, K.-B.; Rossnagel, S. M. Ionic Field Effect Transistors with Sub-10 nm Multiple Nanopores. *Nano Lett.* **2009**, *9*, 2044−2048.
(13) Guan, W.; Fan, R.; Reed, M. A. Field-Effect Reconfigurable Nanofluidic Ionic Diodes. *Nat. Commun.* **2011**, *2*, 506 DOI: 10.1038/ncommns1514(2011).
(14) Guan, W.; Reed, M. A. Electric Field Modulation of the Membrane Potential in Solid-State Ion Channels. *Nano Lett.* **2012**, *12*, 6441−6447.
(15) Macdonald, J. R. Theory of AC Space-Charge Polarization Effects in Photoconductors, Semiconductors, and Electrolytes. *Phys. Rev.* **1953**, *92*, 4−17.
(16) Barbero, G.; Neto, A. M. F.; Freire, F. C. M.; Le Digabel, J. Relaxation Time for the Ionic Current in a Nematic Cell under a Large Electric Field. *Phys. Rev. E* **2006**, *74*, 052701.
(17) Serghei, A.; Tress, M.; Sangoro, J. R.; Kremer, F. Electrode Polarization and Charge Transport at Solid Interfaces. *Phys. Rev. B* **2009**, *80*, 184301.
(18) Andersen, M. B.; van Soestbergen, M.; Mani, A.; Bruus, H.; Biesheuvel, P. M.; Bazant, M. Z. Current-Induced Membrane Discharge. *Phys. Rev. Lett.* **2012**, *109*, 108301.
(19) Simon, P.; Gogotsi, Y. Materials for Electrochemical Capacitors. *Nat. Mater.* **2008**, *7*, 845−854.
(20) Rica, R. A.; Ziano, R.; Salerno, D.; Mantegazza, F.; Brogioli, D. Thermodynamic Relation between Voltage-Concentration Dependence and Salt Adsorption in Electrochemical Cells. *Phys. Rev. Lett.* **2012**, *109*, 156103.
(21) Wei, D.; Scherer, M. R. J.; Bower, C.; Andrew, P.; Ryhänen, T.; Steiner, U. A Nanostructured Electrochromic Supercapacitor. *Nano Lett.* **2012**, *12*, 1857−1862.
(22) Storm, A. J.; van Noort, J.; de Vries, S.; Dekker, C. Insulating Behavior for DNA Molecules between Nanoelectrodes at the 100 nm Length Scale. *Appl. Phys. Lett.* **2001**, *79*, 3881−3883.
(23) Fologea, D.; Uplinger, J.; Thomas, B.; McNabb, D. S.; Li, J. Slowing DNA Translocation in a Solid-State Nanopore. *Nano Lett.* **2005**, *5*, 1734−1737.
(24) Dekker, C. Solid-State Nanopores. *Nat. Nanotechnol.* **2007**, *2*, 209−215.
(25) Tsutsui, M.; He, Y.; Furuhashi, M.; Rahong, S.; Taniguchi, M.; Kawai, T. Transverse Electric Field Dragging of DNA in a Nanochannel. *Sci. Rep.* **2012**, *2*, 394.
(26) Zwolak, M.; Di Ventra, M. Electronic Signature of DNA Nucleotides via Transverse Transport. *Nano Lett.* **2005**, *5*, 421−424.
(27) Lagerqvist, J.; Zwolak, M.; Di Ventra, M. Fast DNA Sequencing via Transeverse Electronic Transport. *Nano Lett.* **2006**, *6*, 779−782.
(28) Lagerqvist, J.; Zwolak, M.; Di Ventra, M. Influence of the Environment and Probes on Rapid DNA Sequencing via Transverse Electronic Transport. *Biophys. J.* **2007**, *93*, 2384−2390.

(29) Szarek, P.; Suwannawong, S.; Doi, K.; Kawano, S. Theoretical Study on Physicochemical Aspects of a Single Molecular Junction: Application to the Bases of ssDNA. *J. Phys. Chem. C* **2013**, *117*, 10809−10817.
(30) Kowalczyk, S. W.; Dekker, C. Measurement of the Docking Time of a DNA Molecule onto a Solid-State Nanopore. *Nano Lett.* **2012**, *12*, 4159−4163.
(31) Butler, J. A. V. The Mechanism of Overvoltage and Its Relation to the Combination of Hydrogen Atoms at Metal Electrodes. *Trans. Fraday Soc.* **1932**, *28*, 379−382.
(32) Wynne-Jones, W. F. K.; Eyring, H. The Absolute Rate of Reactions in Condensed Phases. *J. Chem. Phys.* **1935**, *3*, 492−502.
(33) Butler, J. A. V. Hydrogen Overvoltage and the Reversible Hydrogen Electrode. *Proc. R. Soc. London, Ser. A* **1936**, *157*, 423−433.
(34) Eyring, H.; Glasstone, S.; Laidler, K. J. Application of the Theory of Absolute Reaction Rates to Overvoltage. *J. Chem. Phys.* **1939**, *7*, 1053−1065.
(35) Kimball, G. E. The Absolute Rates of Heterogeneous Reactions II. Electrode Reactions. *J. Chem. Phys.* **1940**, *8*, 199−204.
(36) Laviron, E. The Use of Linear Potential Sweep Voltammetry and of A.C. Voltammetry for the Study of the Surface Electrochemical Reaction of Strongly Adsorbed Systems and of Redox Modified Electrodes. *J. Electroanal. Chem.* **1979**, *100*, 263−270.
(37) Agar, J. N.; Bowden, F. P. The Kinetics of Electrode Reactions. I and II. *Proc. R. Soc. London, Ser. A* **1938**, *169*, 206−234.
(38) Kharkats, Y. I. Theory of the Exaltation Effect and the Effect of Correlation Exaltation of Migration Current. *J. Electroanal. Chem.* **1979**, *105*, 97−114.
(39) Chandrasekhar, S. Stochastic Problems in Physics and Astronomy. *Rev. Mod. Phys.* **1943**, *15*, 1−89.
(40) Kubo, R.; Yokota, M.; Nakajima, S. Statistical-Mechanical Theory of Irreversible Processes. II. Response to Thermal Disturbance. *J. Phys. Soc. Jpn.* **1957**, *12*, 1203−1211.
(41) Schoch, R. B.; Han, J.; Renaud, P. Transport Phenomena in Nanofluidics. *Rev. Mod. Phys.* **2008**, *80*, 839−883.
(42) Bard, A. J.; Faulkner, L. R. *Electrochemical methods*; John Wiley & Sons: New York, 1980.
(43) Hamelin, A. Cyclic Voltammetry at Gold Single-Crystal Surfaces. Part 1. Behavior at Low-Index Faces. *J. Electroanal. Chem.* **1996**, *407*, 1−11.
(44) Sokalski, T.; Lingenfelter, P.; Lewenstam, A. Numerical Solution of the Coupled Nernst−Planck and Poisson Equations for Liquid Junction and Ion Selective Membrane Potentials. *J. Phys. Chem. B* **2003**, *107*, 2443−2452.
(45) Sokalski, T.; Kucza, W.; Danielewski, M.; Lewenstam, A. Time-Dependent Phenomena in the Potential Response of Ion-Selective Electrodes Treated by the Nernst-Planck-Poisson Model. Part 2: Transmembrane Processes and Detection Limit. *Anal. Chem.* **2009**, *81*, 5061−5022.
(46) Lingenfelter, P.; Bedlechowicz-Sliwakowska, I.; Sokalski, T.; Maj-Zurawska, M.; Lewenstam, A. Time-Dependent Phenomena in the Potential Response of Ion-Selective Electrodes Treated by the Nernst-Planck-Poisson Model. 1. Intramembrane Processes and Selectivity. *Anal. Chem.* **2006**, *78*, 6783−6791.
(47) Tabard-Cossa, V.; Trivedi, D.; Wiggin, M.; Jetha, N. N.; Marziali, A. Noise Analysis and Reduction in Solid-State Nanopores. *Nanotechnol.* **2007**, *18*, 305505.
(48) Smeets, R. M. M.; Keyser, U. F.; Dekker, N. H.; Dekker, C. Noise in Solid-State Nanopores. *Proc. Natl. Acad. Sci. U. S. A.* **2008**, *105*, 417−421.
(49) Venkatesan, B. M.; Estrada, D.; Banerjee, S.; Jin, X.; Dorgan, V. E.; Bae, M.-H.; Aluru, N. R.; Pop, E.; Bashir, R. Stacked Graphene−Al_2O_3 Nanopore Sensors for Sensitive Detection of DNA and DNA−Protein Complexes. *ACS Nano* **2012**, *6*, 441−450.
(50) Press, W. H.; Teukolsky, S. A.; Vetterling, W. T.; Flannery, B. P. *Numerical Recipes in Fortran 77*, 2nd ed.; Cambridge University Press: Cambridge, U.K., 1992; pp 279−280.
(51) Vidulich, G. A.; Evans, D. F.; Kay, R. L. The Dielectric Constant of Water and Heavy Water between 0 and 40°. *J. Phys. Chem.* **1967**, *71*, 656−662.